Applied Catalysis B: Environmental 94 (2010) 234–240

Contents lists available at ScienceDirect

Applied Catalysis B: Environmental

journal homepage: www.elsevier.com/locate/apcatb

# Preparation and photodegradation activity of high aspect ratio rutile $TiO_2$ single crystal nanorods

Chunrong Xiong [a,b,c,*], Xiangyun Deng [b,c], Jianbao Li [b,c]

[a] Department of Chemical Engineering, Lab of Petrochemical Technology, Hainan University, Haikou 570228, PR China
[b] Department of Materials, Hainan Provincial Key Laboratory of Research on Utilization of Si-Zr-Ti Resources, Hainan University, Haikou 570228, PR China
[c] Department of Materials, Key Laboratory of Ministry of Education for Application Technology of Chemical Materials in Hainan Superior Resources, Hainan University, Haikou 570228, PR China

ARTICLE INFO

*Article history:*
Received 17 September 2009
Received in revised form 20 November 2009
Accepted 21 November 2009
Available online 27 November 2009

*Keywords:*
Rutile $TiO_2$
High aspect ratio
Well faceted
Single crystal nanorods

ABSTRACT

Well faceted $TiO_2$ nanorods with a regular geometric configuration were hydrothermally prepared by chemical modification of $TiCl_4$ by ethylene glycol to slow down the reactivity of the precursor toward water. XRD patterns revealed that the as made products were pure rutile. The nanorods were highly crystalline and had an elongated prismatic shape. They grew in the [0 0 1] direction and have an aspect ratio of ~45. The rod size can also be tailored via recipe modification. Ag loaded $TiO_2$ was achieved upon exposure of the rutile nanorods to UV light in $AgNO_3$ aqueous solution. The photocatalytic activities of the pure and Ag loaded $TiO_2$ nanorods were evaluated by the photodegradation of phenol and methylene green (MG).



## 1. Introduction

$TiO_2$ has been extensively investigated owing to its notable functions for photocatalysis and photon–electron transfer. Anatase $TiO_2$ has been paid much greater attention than rutile because anatase had been considered to be more active than rutile. Recently, some authors reported that a synergistic effect of anatase and rutile mixed phases may enhance the photocatalytic activity [1–4], while others obtained the best results using pure rutile [5–9]. Deceleration of the electron–hole recombination rate is essential for improving the efficiency of the net charge transfer in photocatalysis [10–12]. Photocatalytic activity of $TiO_2$ is greatly influenced by many factors including specific surface area, crystal structure, crystallite size, morphology, shape, particle aggregation, phase composition, surface defects, and surface hydroxyl group content and so on [13,14]. These factors are strongly related to synthesis and processing routes [13]. Tsai and Cheng [15] compared several commercial and the lab-made $TiO_2$ samples in the photodegradation of phenol and found that the lab-made rutile without thermal annealing showed greatest activities in complete oxidation of phenol to $CO_2$. Upon systematical study of the photocatalytic activity of a variety of hydrothermally prepared $TiO_2$ particles, Testino et al. [13] pointed out that high crystallinity and high aspect ratio are the key parameters to substantially improve the photocatalytic activity of rutile. These findings prompted us to prepare well-crystallized rutile $TiO_2$ nanorods with higher aspect ratio, because carriers can freely move along the length of the rods, which is expected to reduce the electron–hole recombination [12]. Furthermore, nanorods with high aspect ratio and large size are highly desirable as these nanoparticles are easier to be separated in water treatment [16–18].

$TiO_2$ nanocrystals with various morphologies and shapes have been prepared by many methods mainly including electronspining, templating and hydrothermal preparation [19–25]. A distinct advantage of hydrothermal preparation over electrospining or templating fabrication is that the as made product is crystalline, avoiding a thermal annealing step that consequently decreases the surface hydroxyl group content. However, it is relatively difficult to achieve nanorods with high aspect ratio like those obtained with electrospining or templating fabrication by means of hydrothermal preparation. Controlling of the reaction rate is crucial in obtaining $TiO_2$ nanocrystals with the desired crystalline structure and/or shapes [24]. It has been shown that it is possible to modulate the hydrolysis rate by using oleic acid as a stabilizing surfactant to control the growth of $TiO_2$ nanorods, which have an reported aspect ratio of about 11 [12]. Furthermore, lauric acid and trioctylphosphine oxide, surface selective and nonselective surfactant, respectively, have been used to induce the shape evolution

* Corresponding author at: Department of Chemical Engineering, Lab of Petrochemical Technology, Hainan University, Renming Avenue 58, Haikou, PR China. Tel.: +86 898 66279226; fax: +86 898 66271762.
*E-mail address:* bearcr_82@hotmail.com (C. Xiong).

0926-3373/$ – see front matter © 2009 Elsevier B.V. All rights reserved.
doi:10.1016/j.apcatb.2009.11.013

of $TiO_2$ nanocrystals due to the intrinsic anisotropic features of $TiO_2$ [26]. Another instance of surfactant modified reaction rate can be found in the article by Hyeon and co-workers [24], who synthesized $TiO_2$ nanorods with an aspect ratio of 9 using Pluronic P-123 ($EO_{20}PO_{70}EO_{20}$) triblock copolymer to control the hydrolysis and condensation of the titanium tetraisopropoxide (TTIP) precursor. Herein, ethylene glycol was used to stabilize $TiCl_4$ during chemical modification to further enhance the aspect ratio and crystallinity of the $TiO_2$ nanorods. The as made $TiO_2$ nanorods have a higher aspect ratio than those reported previously in the literatures [12,24,26], i.e. 45 and a regular geometric configuration corresponding to rutile crystal, which was rarely seen in the previous reports.

The noble metal nanoparticle may act as a sink aiding electron–hole separation [27–30]. In recent years, noble metal/semiconductor oxide nanocomposites have been recognized to promote photocatalysis [10,31–33]. Ag modified $TiO_2$ has been prepared by various methods including precipitation deposition, incipient wet-impregnation, sol–gel method, MOCVD, and photoreduction under ultraviolet irradiation [34–36]. To maximize the efficiency of photocatalytic reactions on the as made $TiO_2$ nanorods, the nanorods were loaded with Ag through photoreduction of $AgNO_3$ under ultraviolet exposure.

## 2. Experimental

### 2.1. Synthesis of $TiO_2$ single crystal nanorods

In synthesis of sample A, 0.5 ml of $TiCl_4$ was dissolved in 12 ml of ethylene glycol under stirring, then 4.5 ml of 25% $BaCl_2$ aqueous solution was added at room temperature. The solution was clear and transparent probably owing to relative stability of the intermediate produced from the reaction of ethylene glycol with $TiCl_4$ as described in the following equation. The mixture was vigorously stirred for 1.5 h, and then transferred into a 20 ml Teflon-lined autoclave for hydrothermal treatment at 145 °C for 48 h. The precipitate was isolated by vacuum filtration, washed with acetone followed by deionized water, several additional $TiO_2$ samples were also prepared in the similar strategy.

### 2.2. Preparation of Ag loaded $TiO_2$ nanorods

The Ag loaded $TiO_2$ catalysts were prepared by photoreducing $Ag^+$ ions to Ag on the $TiO_2$ surface as described in the literature [37]. 0.5 g of $TiO_2$ nanorods were suspended in 50 ml of 0.2 M $AgNO_3$ aqueous solution. The pH of the solution was adjusted to 3 with 1 M nitric acid. The mixture was exposed to air in a chamber and irradiated with UV light by eight mercury lamps (8 W) for 2 h under magnetically stirring. The Ag loaded $TiO_2$ was filtered and washed with DI water. The atomic ratio of Ag to Ti was determined using EDS analysis with Genesis microanalysis software combining energy-dispersive analysis of X-ray spectroscopy (EDS) algorithms for standardless quantification.

### 2.3. Characterization

The crystallinity of the $TiO_2$ was determined by powder X-ray diffraction (XRD) (Scintag XDS 2000 X-ray diffractometer with Cu Kα radiation). The BET specific surface areas were determined on a Gemini V2365 porousimetry analyzer using $N_2$ adsorption–desorption. The morphology was evaluated by scanning electron microscopy (LEO 1530 VP field emission SEM) from Au/Pd coated samples. The microstructure was observed by transmission electron microscopy (TEM) using an FEI CM200 FEG transmission electron microscope at 200 kV.

### 2.4. Photodegradation of phenol

The photoreactor was a 100 ml cylindrical Pyrex flask, illuminated at the bottom through a 12 $cm^2$ of optical window illuminated by a HPM 500 W high-pressure mercury lamp through a water filter. The intensity of light reaching the photoreactor was 22 $mW/cm^2$ measured with a radiometer. Photodegradation of phenol was performed at room temperature. For all experiments, 15 mg of catalyst was dispersed in 70 ml of 300 ppm phenol aqueous solution with an oxygen flow of 10 ml $min^{-1}$. Before the reaction, the suspension was mechanically stirred for 30 min in a dark environment. The unreacted phenol was analyzed by high-pressure liquid chromatography (HP 1090). A column (ODS Hypersil 5 μm, 100 mm × 4.6 mm) with methanol/water (30/70, 0.4 ml/min) as an eluent was used. Detection was conducted by a UV detector at 280 nm.

### 2.5. Decolorization of dyes

The photocatalytic activities of the $TiO_2$ nanorods were also evaluated in photocatalytic decolorization of methylene green (MG, the dye content is ca. 65%). The initial MG concentration was $2.8 \times 10^{-5}$ M with an initial pH of 5.6. For all experiments, the reaction solution contained 25 mg of catalyst and 70 ml of dye solution. The suspension was magnetically stirred in a dark environment at room temperature for 30 min to establish an adsorption–desorption equilibrium. The catalytic reactions were carried out using the same photoreactor and light source as stated in the photodegradation of phenol. The concentrations of MG at different intervals were calculated from UV–vis absorption spectra at 657.5 nm, the band corresponding to MG.

## 3. Results and discussion

The $TiCl_4$ dissolved in ethylene glycol was bright yellow in color possibly due to the formation of an ethylene glycol chelated Ti. The solution maintained clear even if $BaCl_2$ aqueous solution was added, which indicated that the intermediate was relatively stable to water at room temperature. Five different $TiO_2$ samples were prepared in the similar strategy for this study. The preparation recipes of the samples were summarized in Table 1. During the syntheses, the amounts of the $TiCl_4$, ethylene glycol and $BaCl_2$ were varied in the initial mixture to determine the influence of the reactant composition on the morphology of $TiO_2$ nanoparticles. XRD patterns in Fig. 1 reveal that a pure rutile phase was generated

**Table 1**
Summary of recipes and BET specific surface areas for different $TiO_2$ nanorod samples.

| Sample | $TiCl_4$ (ml) | Ethylene glycol (ml) | 25% $BaCl_2$ aqueous solution (ml) | Deionic water (ml) | BET surface areas of the $TiO_2$ rods ($m^2/g$) |
|---|---|---|---|---|---|
| Sample A | 0.5 | 12 | 4.5 | 0 | 42 |
| Sample B | 0.5 | 24 | 4.5 | 0 | 51 |
| Sample C | 0.5 | 12 | 0 | 3.5 | 44 |
| Sample D | 0.5 | 24 | 0 | 3.5 | 54 |
| Sample E | 0.5 | 0 | 4.5 | 12 | 53 |

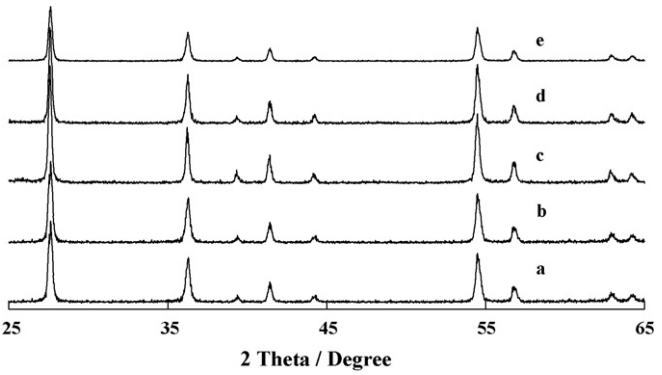


**Fig. 1.** XRD patterns of the $TiO_2$ nanorods, (a)–(e) correspond to the samples A–E, respectively.

for the five samples under the autogenous acidic condition, since an acidic environment favors the corner-shared bonding and formation of rutile phase [13].

Fig. 2 displays SEM images of samples A–D. The $TiO_2$ nanocrystals of the four samples grow uniaxially, resulting in a rod-like morphology. Sample A consists of $TiO_2$ nanorods with a typical rutile crystal shape, an elongated prismatic configuration as seen from the SEM images in Fig. 2a and b. The high resolution SEM image in Fig. 2b exhibits that the nanorods are well faceted and have a sharp geometric configuration, which are indicative of a good crystallization. The rods have a relatively uniform length up to 2 μm and width of 45 nm. For the sample prepared with the lower $TiCl_4$/ethylene glycol ratio, B, the rod sizes were decreased to 22 nm in width and 1 μm in length as shown in Fig. 2c and d. In terms of the two samples, the rods have an aspect ratio of about 45. BET specific surface areas of the samples A and B are 42 and 51 $m^2$/g, respectively. For the samples without the addition of $BaCl_2$ in the reactant mixture, debris was found on the rod surface as shown in Fig. 2e and f. In contrast, the rod surfaces of the samples A and B are very clean and smooth. For the samples C and D, BET specific surface areas are 44 and 54 $m^2$/g, respectively, which are a little higher than those of the samples A and B correspondingly, probably because of formation of the debris spots on the rod surfaces. Sample E, prepared without ethylene glycol, did not exhibit a rod-like morphology (as seen in Fig. S1) due to immediate hydrolysis of $TiCl_4$ in water.

Furthermore, it can be observed in the Fig. 2a, b and e that small amount of rutile nanorods twins with each other at an angle of 120°, forming "knee" shaped twins as highlighted with circles. Twinning occurs when two crystals appear to be growing out of (or into) each other as a result of an error during the crystallization

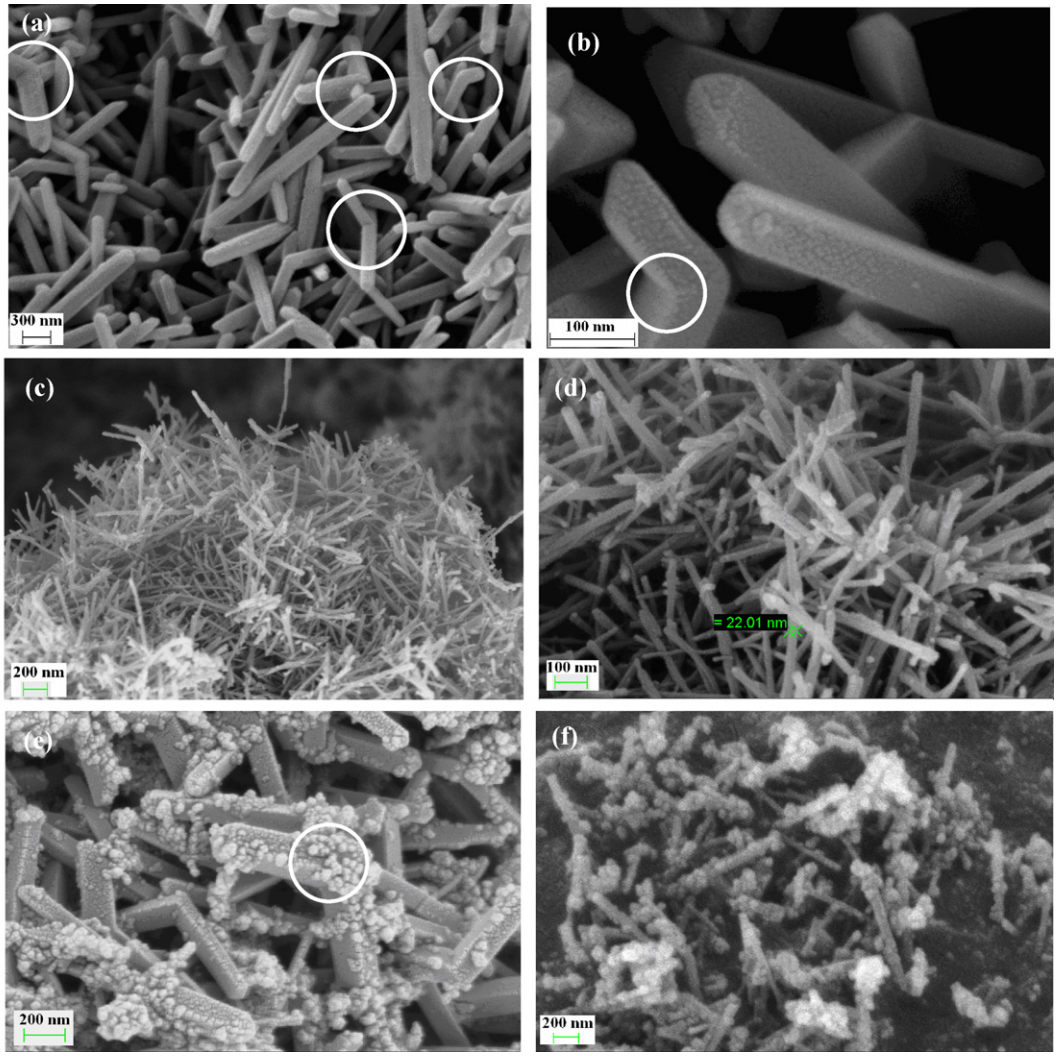


**Fig. 2.** SEM images of the $TiO_2$ nanorods, (a) and (b) correspond to the sample A, (c) and (d) correspond to the sample B, (e) and (f) correspond to the samples C and D, respectively.

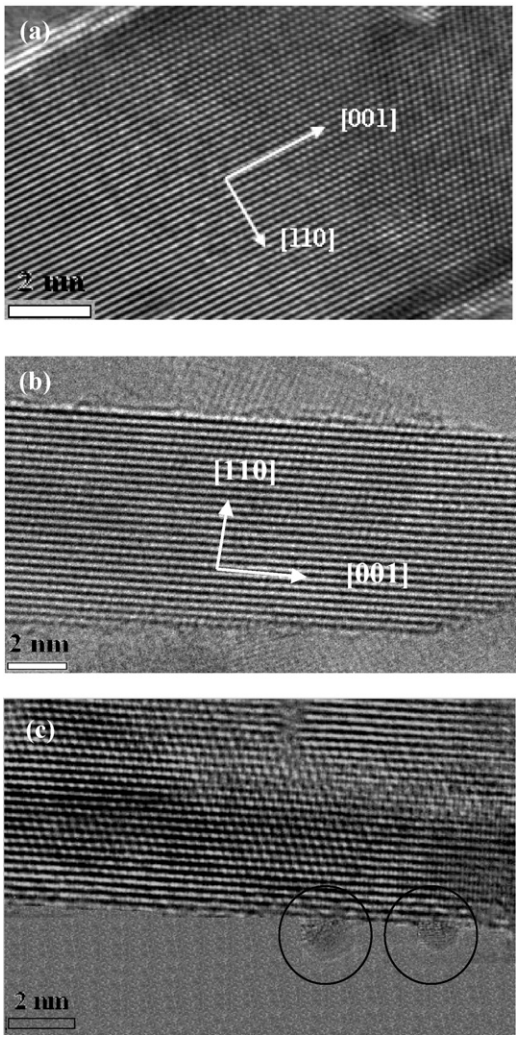


**Fig. 3.** HRTEM images of $TiO_2$ nanorods, (a) the sample A, (b) the sample B, and (c) the sample C.

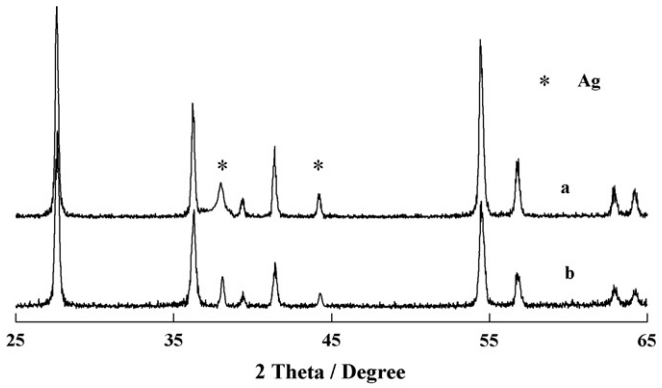


**Fig. 4.** XRD patterns of (a) the Ag loaded sample A, and (b) the Ag loaded sample B.

process. The HRTEM images in Fig. 3 further confirm that the nanorods are highly crystalline rutile. The lattice fringes of (1 1 0) planes show a *d*-spacing of 3.24 Å, and the nanorods grow in the [0 0 1] direction, which indicates that the growth of [0 0 1] direction is faster than the [1 1 0] direction. The predominant growth direction of [0 0 1] also agrees with rutile's inherent growth habit that was described in the reports [38–40]. The structure of rutile consists of $TiO_6$ octahedra chains, in which each octahedron shares a pair of opposite edges in the (0 0 1) plane. The debris spots were thought to be amorphous due to no fringes observed in the TEM image as shown in Fig. 3c.

Hydrolysis and polycondensation are two major factors affecting the growth and crystallinity of $TiO_2$. The precursor $TiCl_4$ is known to readily react with water, whereas chelation of Ti by ethylene glycol appears to slow down the hydrolysis and force it to proceed slowly in the autoclave. At an early stage, partial hydrolysis primarily led to monoethylene glycol chelated $TiO_6$ octahedra. These organic modified $TiO_6$ monomers subsequently protonated and condensed under the acidic condition, giving rise to titania aggregation and nucleation as illustrated in Scheme 1. The Ti–O–Ti framework cores were surrounded by a hydrocarbon periphery, which is similar to the picture described by Weller and co-workers [12]. Cross growth of Ti–O–Ti framework is thus

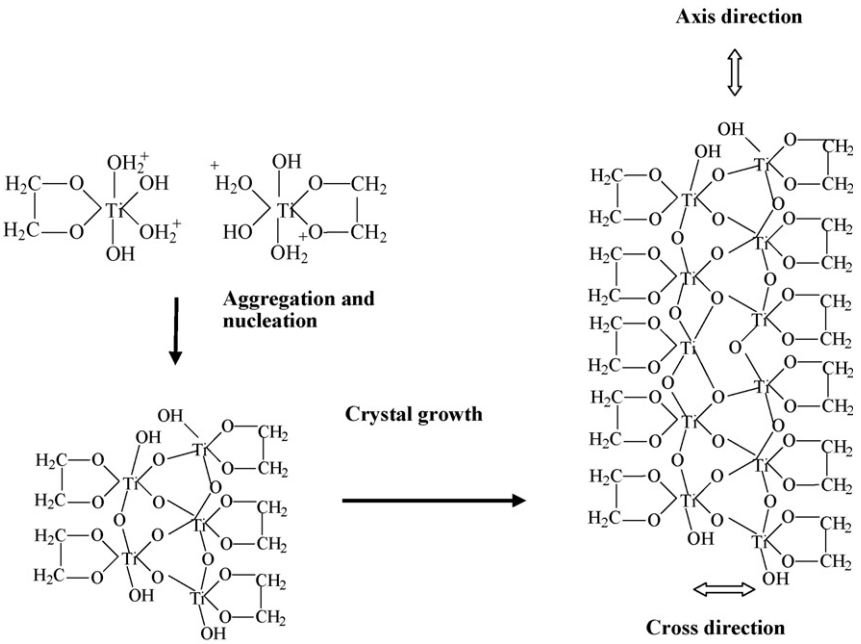


**Scheme 1.** The formation process of the rod-like $TiO_2$.

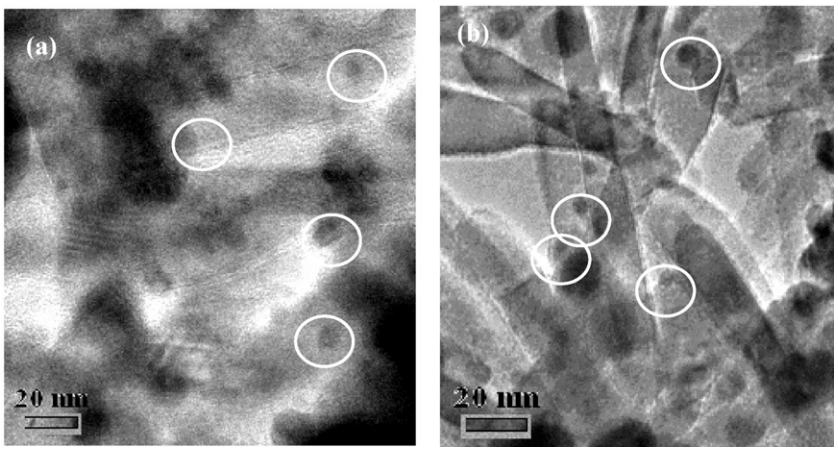


**Fig. 5.** TEM images of (a) the Ag loaded sample A, and (b) the Ag loaded sample B.

limited by the protection of the alkoxy groups. Consequently, the cores have a propensity to extend toward both ends, resulting in a rod-like morphology. The $TiO_2$ rods do not grow along the cross direction until the surrounding alkoxy groups are allowed to hydrolyze with longer autoclaving time. We assume that hydrolysis rate of the second alkoxy controls the width of the nanorods, and the condensation rate is relevant to the length. Therefore, the two rates are the most influential factors in structure and shape control, and the ratio of the rates determines the aspect ratio of the rods to some extent.

Sample B, containing an amount two times the ethylene glycol used relative to the sample A in the initial mixture, has smaller rod sizes but nearly the same aspect ratio. Ethylene glycol diluted the Ti precursor and water at the same time, which proportionately decreased the condensation rate and the hydrolysis rate of the second alkoxy. This means that the ratio of the condensation rate to the hydrolysis rate was the same for samples A and B, hence the dilution effect of ethylene glycol would not significantly affect the rod aspect ratio. The slower condensation rate and the slower hydrolysis rate could lead to generation of more nuclei in sample B with respect to sample A, which resulted in smaller rod sizes. For the samples C and D, the amorphous debris on the rod surfaces might be ascribed to a slow nucleation process in the absence of $BaCl_2$ [41]. Presence of the cation $Ba^{2+}$ may enhance the rutile nucleation and growth, which is in good agreement with the parallel reports [42,43]. In addition, the $Cl^-$ anion was also reported to enhance the nucleation [44]. The nucleophilic substitution of the chloride anion to the $TiO_6$ octahedra produced the chloride atom-substituted octahedral similar to the partially hydrolyzed $Ti(OH)_nCl_m$. More $Cl^-$ in the complex would be beneficial to the formation of the rutile phase [41,44,45].

Metallic silver may act as an electron trap, thereby enhancing the electron–hole pair separation and slowing the electron–hole recombination. To improve the photocatalysis activities of the rutile $TiO_2$ nanorods, the samples A and B were loaded with the Ag metal by photoreducing $Ag^+$ ions. The XRD patterns in Fig. 4 display the characteristic peaks of the Ag metal and indicated the presence of Ag in both samples. The metal Ag particles, as denoted by circles, can also be observed from the TEM images in Fig. 5. The atomic ratio of Ag to Ti for both samples was about 5.1% determined using EDS analysis. According to the literatures [15,34,35,46], the optimum Ag/Ti atomic ratio for photocatalysis was reported to be in the range of 2–6%.

The photocatalytic activities of the rutile $TiO_2$ nanorods were evaluated by photooxidation experiments of phenol. For comparison, Degussa P-25, the most commonly used $TiO_2$-based photocatalyst (30 nm $TiO_2$ nanoparticles having a surface area of $\sim$50 $m^2/g$), was examined in the same photocatalytic reactions. The results are shown in Fig. 6. The half transformation time of phenol, $t_{1/2}$, is taken as a representative parameter to compare the degradation rates. The $t_{1/2}$ value decreases with the maximum degradation rate according to the previous report [13]. The $t_{1/2}$ values for different catalysts were read from the curves in Fig. 6. An apparent order of photocatalytic activities is as follows: the Ag loaded samples A and B > the samples A and B > Degussa P-25, the samples C and D > the sample E. The samples A and B exhibited much higher photocatalytic activities than Degussa P-25, which supports the previous reports that desirability of the rutile phase is

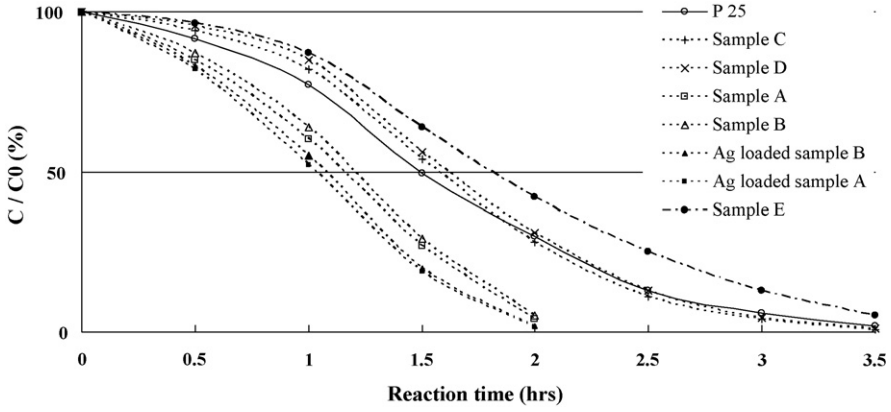


**Fig. 6.** Plot of percent conversion vs time for the photodegradation of phenol on rutile $TiO_2$ nanorods and P-25.

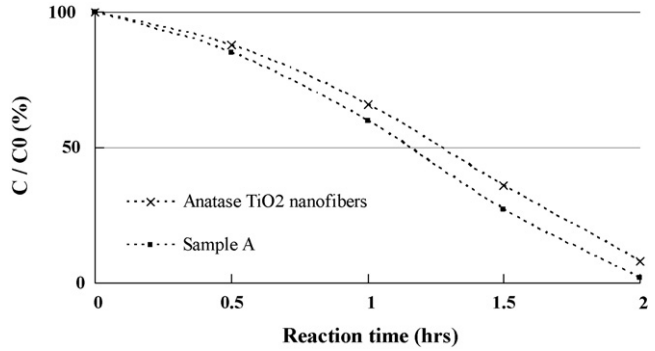


**Fig. 7.** Plot of percent conversion vs time for the photodegradation of phenol on the sample A and hollow anatase $TiO_2$ nanofiber shells.

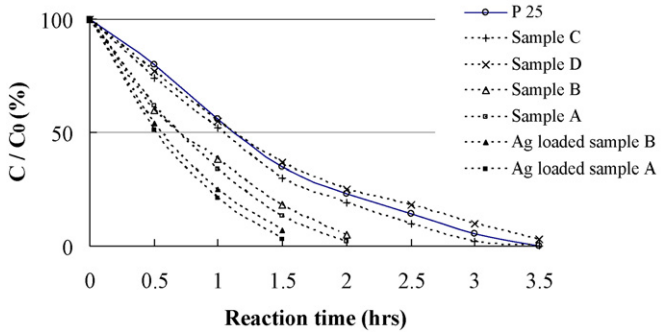


**Fig. 8.** Plot of conversion vs time for the photodegradation of MG on rutile $TiO_2$ nanorods and P-25.

comparable to the other phase composition in photocatalysis [1–5,13,15]. However, the sample C and sample D did not show better photocatalytic activities than P-25, possibly because the partial active sites on the rod surfaces were covered with amorphous particles. In terms of the sample E, the slowest degradation rate further demonstrated that the rod-like morphology, especially with high aspect ratio, is important for reducing the electron–hole recombination.

Compared with the pure $TiO_2$ rutile nanorods of the sample A and sample B, the Ag loaded ones have an increase of ~12% in the photodegradation activity, indicating that the dopant Ag can suppress the recombination of electron–hole pairs to some extent and increase photodegradation efficiency. Generally, the rods with smaller sizes have a higher surface to volume ratio, favoring the photocatalytic activity. However, the sample B with smaller rod sizes than those of the sample A, did not present an increased photodegradation rate. This is consistent with the previous observation by Testino et al. [13]. For a given aspect ratio, the electron–hole pair recombination is slower in the well faceted and bigger rutile $TiO_2$ particles, thus promoting a higher activity, despite the decrease of the specific surface area [13].

To make comparative reference to anatase, $TiO_2$ nanofibers with diameter of ~25 nm were prepared from mesoporous silica spheres according to a previously published report [20]. The specific surface area of the $TiO_2$ nanofibers is 46 $m^2/g$. Their SEM images and XRD pattern are shown in Figs. S2 and S3, respectively. The fibers are anatase and polycrystalline [20]. Fig. 7 shows the results for the photodegradation of phenol catalyzed by the anatase nanofibers and the rutile nanorods under the same reaction conditions. It can be seen that the rutile nanorods displayed a faster photocatalysis reaction rate as compared to the anatase $TiO_2$ nanofibers, which indicated that the well faceted rutile single crystal nanorods can more effectively suppress the recombination of electron–hole pairs and increase photodegradation efficiency compared to the anatase polycrystalline fibers.

In addition to phenol, the dye MG was also investigated as a substrate for photodegradation over the rutile $TiO_2$ nanorods. The results are shown in Fig. 8. The overall trend of the activities is very similar to that observed in the phenol photodegradation. In the photodegradation of MG, the samples A and B still presented higher photocatalytic activities than P-25. Likewise, the sample A showed a better photodegradation activity than the sample B, despite the fact that the sample B has a smaller rod size. As compared to the unloaded $TiO_2$ nanorods, the Ag loaded $TiO_2$ nanorods also exhibited a better activity. The time to completely bleach MG was 1.5 h on the Ag loaded samples, half an hour faster than the pure $TiO_2$.

## 4. Conclusions

In summary, well faceted $TiO_2$ single crystal nanorods have been hydrothermally prepared by chelating $TiCl_4$ with ethylene glycol to modulate the hydrolysis rate. Chemical modification of $TiCl_4$ by ethylene glycol was proven to be a rational strategy to tune the reactivity of the precursor toward water and produce the anisotropic Ti–O–Ti nuclei, leading to a shape control growth of $TiO_2$ particles. The as made $TiO_2$ nanorods were in the rutile phase and had an elongated prismatic rutile crystal shape with an aspect ratio of 45. The addition of $BaCl_2$ in the reactant mixture might enhance the $TiO_2$ nucleation and growth, effectively avoiding the formation of amorphous particles during the crystallization process. In the photodegradation of phenol and MG, well-crystallized rutile $TiO_2$ nanorods exhibited better catalytic activities than the partially crystallized ones and P-25. Additionally, the well faceted rutile $TiO_2$ nanorods with high aspect ratio could have a further application in the deep mineralization of recalcitrant organics. Ag loading may further suppress the recombination rate of the electron–hole pairs, which was demonstrated in our photodegradation reactions.

## Acknowledgement

The authors would like to acknowledge the Hainan University for financing this work.

## Appendix A. Supplementary data

Supplementary data associated with this article can be found, in the online version, at doi:10.1016/j.apcatb.2009.11.013.

## References

[1] R.R. Bacsa, J. Kiwi, Appl. Catal. B 16 (1998) 19.
[2] D. Gumy, C. Morais, P. Bowen, C. Pulgarin, S. Giraldo, R. Hajdu, J. Kiwi, Appl. Catal. B 63 (2006) 76.
[3] S. Watson, D. Beydoun, J. Scott, R. Amal, J. Nanopart. Res. 6 (2004) 193.
[4] M. Yan, F. Chen, J. Zhang, M. Anpo, J. Phys. Chem. B 109 (2005) 8673.
[5] S.S. Watson, D. Beydoun, J.A. Scott, R. Amal, Chem. Eng. J. 95 (2003) 213.
[6] A. Mills, S.K. Lee, A. Lepre, J. Photochem. Photobiol. A 155 (2003) 199.
[7] M.H. Habibi, H. Vosooghian, J. Photochem. Photobiol. A 174 (2005) 45.
[8] D.D. Beck, R.W. Siegel, J. Mater. Res. 7 (1992) 2840.
[9] T. Ohno, D. Haga, K. Fujihara, K. Kaizaki, M. Matsumura, J. Phys. Chem. B 101 (1997) 6415.
[10] N. Sobana, M. Muruganadham, M. Swaminathan, J. Mol. Catal. A: Chem. 258 (2006) 124.
[11] J.M.J. Laine, J.M. Herrmann, Appl. Catal. B 18 (1998) 281.
[12] P.D. Cozzoli, A. Kornowski, H. Weller, J. Am. Chem. Soc. 125 (2003) 14539.
[13] A. Testino, I.R. Bellobono, V. Buscaglia, C. Canevali, M. D'Arienzo, S. Polizzi, R. Scotti, F. Morazzoni, J. Am. Chem. Soc. 129 (2007) 3564.
[14] J. Yu, J. Xiong, B. Cheng, S. Liu, Appl. Catal. B 60 (2005) 211.
[15] S.J. Tsai, S.F. Cheng, Catal. Today 33 (1997) 227–237.

[16] C.E. Bonancêa, G.M. do Nascimento, M.L. de Souza, M.L.A. Temperini, P. Corio, Appl. Catal. B: Environ. 69 (2006) 34–42.
[17] R. Comparelli, E. Fanizza, M.L. Curri, P.D. Cozzoli, G. Mascolo, A. Agostiano, Appl. Catal. B: Environ. 60 (2005) 1–11.
[18] S. Mozia, M. Tomaszewska, A.W. Morawski, Appl. Catal. B: Environ. 59 (2005) 131–137.
[19] C.R. Xiong, K.J. Balkus Jr., Chem. Mater. 17 (2005) 5136.
[20] C.R. Xiong, M.J. Kim, K.J. Balkus Jr., Small 2 (2006) 52.
[21] F. Bosc, A. Ayral, P. Albouy, C. Guizard, Chem. Mater. 15 (2003) 2463.
[22] M. Niederberger, M.H. Hartl, G.D. Stucky, Chem. Mater. 14 (2002) 4364.
[23] D.P. Serrano, G. Calleja, R. Sanz, P. Pizarro, Chem. Commun. (2004) 1000.
[24] S. Han, S.H. Choi, S.S. Kim, M. Cho, B. Jang, D.Y. Kim, J. Yoon, T. Hyeon, Small 1 (2005) 812.
[25] K. Nagaveni, G. Sivalingam, M.S. Hegde, G. Madras, Appl. Catal. B 48 (2004) 83.
[26] Y.W. Jun, M.F. Casula, J.H. Sim, S.Y. Kim, J. Cheon, A.P. Alivisatos, J. Am. Chem. Soc. 125 (2003) 15981.
[27] A. Sclafani, J.M. Herrmann, J. Photochem. Photobiol. A: Chem. 113 (1998) 181.
[28] A. Wold, Chem. Mater. 5 (1993) 280.
[29] V. Subramanian, E. Wolf, P. Kamat, J. Phys. Chem. B 105 (2001) 11439.
[30] B.E. Hayden, A. King, M.A. Newton, N. Yoshikawa, J. Mol. Catal. A: Chem. 167 (2001) 33.
[31] S. Sena, S. Mahantya, S. Roya, O. Heintzb, S. Bourgeoisb, D. Chaumont, Thin Solid Films 474 (2005) 245.
[32] J.M. Herrmanna, H. Tahiria, Y. Ait-Ichoub, G. Lassalettac, A.R. Gonzilez-Elipe, A. Fernbdez, Appl. Catal. B 13 (1997) 219.
[33] H. Tada, K. Teranishi, S. Ito, Langmuir 15 (1999) 7084.
[34] X. Zhang, M. Zhou, L. Lei, Mater. Chem. Phys. 91 (2005) 73.
[35] C. He, Y. Yu, X.F. Hu, A. Larbot, Appl. Surf. Sci. 200 (2002) 239.
[36] A. Dobosz, A. Sobczynski, Water Res. 37 (2003) 1489.
[37] V. Vamathevan, R. Amal, D. Beydoun, G. Low, S. McEvoy, J. Photochem. Photobiol. A: Chem. 148 (2002) 233.
[38] K. Yang, J. Zhu, J. Zhu, S. Huang, X. Zhu, G. Ma, Mater. Lett. 57 (2003) 4639.
[39] W.J. Li, E.W. Shi, Z.W. Yin, J. Cryst. Growth 208 (2000) 546.
[40] P. Peng, X. Liu, C. Sun, J. Ma, W. Zheng, J. Solid State Chem. 182 (2009) 1003.
[41] H. Yin, Y. Wada, T. Kitamura, S. Kambe, S. Murasawa, H. Mori, T. Sakata, S. Yanagid, J. Mater. Chem. 11 (2001) 1694.
[42] F.D. Duminica, F. Maury, R. Hausbrand, Surf. Coat. Technol. 201 (2007) 9304.
[43] P. Evans, T. English, D. Hammond, M.E. Pemble, D.W. Sheel, Appl. Catal. A: Gen. 321 (2007) 140.
[44] K. Yanagisawa, J. Ovenstone, J. Phys. Chem. B 103 (1999) 7781.
[45] H. Cheng, J. Ma, Z. Zhao, L. Qi, Chem. Mater. 7 (1995) 663.
[46] Y. Cao, H. Tan, T. Shi, T. Tang, J. Li, J. Chem. Technol. Biotechnol. 83 (2008) 546–552.